Research Article

Pattern self-referenced single-pixel computational holographic imaging

Wenjing Zhao,[a,†] Zefang Gao,[a,†] Zhiheng Du,[a] Aiping Zhai,[a] and Dong Wang[a,b,*]
[a]Taiyuan University of Technology, College of Physics and Optoelectronics, Yingze, China
[b]Taiyuan University of Technology, Ministry of Education, Key Laboratory of Advanced Transducers and Intelligent Control System, Yingze, China

Abstract. We propose pattern self-referenced single-pixel common-path holography (PSSCH), which can be realized using either the digital-micromirror-device (DMD) based off-axis scheme or the DMD-based phase-shifting approach, sharing the same experimental setup, to do wavefront reconstructions. In this method, each modulation pattern is elaborately encoded to be utilized to not only sample the target wavefront but also to dynamically introduce the reference light for single-pixel common-path holographic detection. As such, it does not need to intentionally introduce a static reference light, resulting in it making full use of the pixel resolution of the modulation patterns and suppressing dynamically varying noises. Experimental demonstrations show that the proposed method can not only obtain a larger field of view than the peripheral-referenced approach but also achieve a higher imaging resolution than the checkerboard-referenced approach. The phase-shifting-based PSSCH performs better than the off-axis-based PSSCH on imaging fidelity, while the imaging speed of the latter is several times faster. Further, we demonstrate our method to do wavefront imaging of a biological sample as well as to do phase detection of a physical lens. The experimental results suggest its effectiveness in applications.

1 Introduction

Amplitude and phase are critical in applications, such as biomedical imaging,[1] scattering imaging,[2,3] holographic display,[4,5] and microscopy,[6] whereas existing detectors can only record intensity information. In 1948, Gabor historically proposed the first quantitative technique[7] to reconstruct complex light fields using intensity information detected through interference. This pioneering work laid the foundation for modern holography. Subsequently, interference-based holographic imaging technology[8–16] catalyzed the emergence of various research disciplines. In recent years, advancements in detector technology have further expanded its application scope.

In contrast to conventional array detectors featuring extensive pixel arrays,[17] single-pixel detectors utilize structured spatial illumination to achieve spatial sampling through single-point detection.[18–27] This configuration offers distinct advantages, including heightened sensitivity, high dynamic range, and cost-effectiveness. Moreover, single-pixel detectors demonstrate robust performance across a broad spectral range, spanning infrared,[28–31] terahertz,[32–34] and X-ray[35] bands, especially in areas where array detectors are unavailable.

To extract the complex amplitude (i.e., wavefront) of an unknown light field using the single-pixel imaging technique, one of the most effective methods involves employing a holographic approach with an additional reference beam, also known as single-pixel holography (SH). Since 2008, researchers have implemented SH techniques in the framework of single-pixel dual-path interference, including the introduction of phase-shifting modulation using a liquid crystal spatial light modulator (LCSLM) or a digital micromirror device (DMD) in the Mach–Zehnder interferometer[36–38] or Michelson interferometer.[39] However, the dual-path system is generally complex and less stable, making it vulnerable to external environmental interference. To further enhance the imaging performance of SH, single-pixel common-path holography (SCH) techniques have been demonstrated, which are typically realized using a

---

LCSLM[40–45] or DMD.[46–50] However, the modulation bases in the above SCH methods are only used as spatial sampling and additional reference strategies need to be designed to introduce the necessary phase difference for the interference, such as the state-of-the-art checkerboard-referenced[47–49,51] and peripheral-referenced.[41] The former involves dividing the unknown field into signal and reference parts using the checkerboard, which unfortunately leads to a reduction in the spatial imaging resolution. The latter approach employs peripheral pixels to introduce reference light, inevitably sacrificing the peripheral field of view (FOV). Such configurations inevitably lead to a trade-off between imaging spatial resolution and FOV.

Here, a pattern self-referenced single-pixel common-path holography (PSSCH)-based wavefront imaging method is proposed and demonstrated. In the approach, the modulation pattern simultaneously samples the unknown fields and introduces the reference light for the single-pixel common-path holographic detection, eliminating the need for additional reference strategies. This allows us to fully utilize the pixel resolution of the modulation patterns, thereby overcoming the trade-off between the FOV and imaging resolution present in state-of-the-art reference methods. Experimentally, we conduct wavefront reconstruction using the DMD-based off-axis scheme and phase-shifting scheme in the same experimental setup. We then explore its application in wavefront imaging of a biological sample and quantitative imaging for lens phase detection.

2 Principle

In this section, we elucidate the principle of the proposed PSSCH and describe its implementation in both off-axis-based and phase-shifting-based schemes. The modulation bases employed for spatial sampling can be a random basis,[44,52] or orthogonal bases, such as Hadamard basis,[39] Fourier basis,[22,26] and discrete cosine transform (DCT) basis.[47]

2.1 Off-Axis-Based PSSCH

Figure 1 shows the schematic diagram of off-axis-based PSSCH. The sampling patterns $P_n(\vec{r})$ with a spatial resolution $\sqrt{N} \times \sqrt{N}$ are shown in Fig. 1(a), where $n \in [1, N]$. An oblique phase grating $G(\vec{r}) = \exp[i\theta(\vec{r})]$ is designed to introduce the necessary phase difference for the off-axis interference, where i is the imaginary unit and $\theta(\vec{r})$ is the oblique phase (In our following experiments, the angle of the oblique phase grating is 0.67 deg). The amplitude and phase distributions of the oblique phase grating are shown in Fig. 1(b). Then, the encoded patterns are obtained by elaborately superposing sampling patterns with oblique phase grating, as shown in Fig. 1(c). It is worth noting that each encoded pattern $E_n(\vec{r})$ is not only utilized as the spatial sampling pattern but is also used to introduce the phase difference for off-axis interference. Figure 1(d) shows a target wavefront $O(\vec{r})$, where the amplitude is restricted in a circle and the phase is represented by a gray-scale "house" image. After the target wavefront is modulated by an encoded pattern, the resulting modulated wavefront is shown in Fig. 1(e).

Then, the off-axis interference intensity is collected by a lens and detected by a single-pixel detector [Fig. 1(f)], which can be expressed as

$$
\begin{aligned}
y_n &= |\text{FFT}\{E_n(\vec{r}) \cdot O(\vec{r})\}_{\vec{w}=0}|^2 \\
&= \left| \iint P_n(\vec{r}) \cdot O(\vec{r}) d^2\vec{r} + \iint G(\vec{r}) \cdot O(\vec{r}) d^2\vec{r} \right|^2 \\
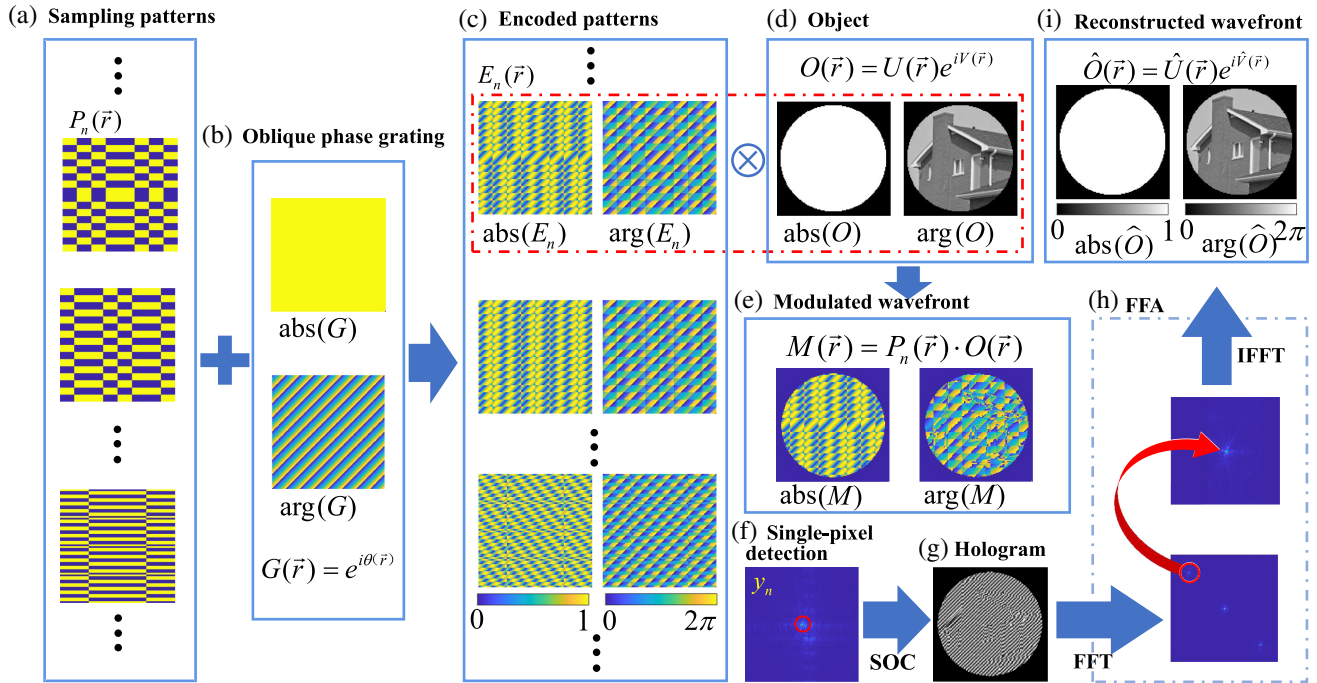&= |S_n + C_1|^2,
\end{aligned} \tag{1}
$$

Fig. 1 The schematic diagram of the off-axis-based PSSCH method. (a) Sampling patterns; (b) oblique phase grating; (c) encoded patterns; (d) target wavefront; (e) modulated wavefront; (f) single-pixel detection; (g) reconstructed hologram; (h) Fourier fringe analysis (FFA); (i) reconstructed wavefront.

where FFT{} represents the two-dimensional Fourier transform, $\vec{r}$ represents the spatial coordinate vector, and $\vec{w}$ is the transform domain coordinate vector. $\vec{w} = 0$ denotes taking the zero-frequency component, $S_n = \iint P_n(\vec{r}) \cdot O(\vec{r}) \mathrm{d}^2\vec{r}$, and $C_1 = \iint G(\vec{r}) \cdot O(\vec{r}) \mathrm{d}^2\vec{r}$, which is a complex constant. The final off-axis hologram can be reconstructed via a second-order correlation (SOC) algorithm, as shown in Fig. 1(g), which can be expressed as

$$H(\vec{r}) = \frac{1}{N}\sum_{n=1}^{N} P_n(\vec{r}) \cdot y_n$$
$$= \frac{1}{N}\sum_{n=1}^{N} P_n(\vec{r})(|S_n|^2 + |C_1|^2) + C_1^* \cdot \hat{O}(\vec{r}) + C_1 \cdot [\hat{O}(\vec{r})]^*,$$

(2)

where $*$ means taking the complex conjugate, $\frac{1}{N}\sum_{n=1}^{N} P_n(\vec{r})(|S_n|^2 + |C_1|^2)$ represents the autocorrelation, and $C_1^* \cdot \hat{O}(\vec{r})$ and $C_1 \cdot [\hat{O}(\vec{r})]^*$ are the complex conjugate cross-correlation terms. According to the Fourier fringe analysis,[53] the spectrum of the off-axis interferogram can be obtained following the Fourier transform. Subsequently, only the first-order component in the Fourier spectrum is extracted and translated to the center of the Fourier spectrum, as demonstrated in Fig. 1(h).

Finally, the reconstructed target wavefront $\hat{O}(\vec{r})$ can be obtained by conducting the inverse Fourier transform using the extracted Fourier spectrum; the amplitude and phase of the reconstructed wavefront are shown in Fig. 1(i). More details on the mathematical derivation of the method are given in Sec. 1 of the Supplementary Material.

2.2 Phase-Shifting-Based PSSCH

Figure 2 shows the schematic diagram of the phase-shifting-based PSSCH. The sampling patterns $[P_n(\vec{r}), n \in [1, N]]$ with a spatial resolution $\sqrt{N} \times \sqrt{N}$ are shown in Fig. 2(a). To achieve the required phase-shifting interference, four steps of phase shiftings, denoted as $R_\alpha = e^{-i\alpha}$, $(\alpha = 0, \frac{\pi}{2}, \pi, \frac{3\pi}{2})$, as shown in Fig. 2(b), are encoded into the sampling patterns, and thus the self-referenced patterns $[E_{n,\alpha}(\vec{r}), n \in [1, N]]$ can be obtained, as shown in Fig. 2(c). As such, each encoded pattern can be utilized not only to spatially sample the target shown in Fig. 2(d) but also to introduce the necessary four steps of phase shiftings. The wavefront of the target object is modulated by the encoded patterns, which gives the modulated wavefront, as shown in Fig. 2(e). The phase-shifting interference intensity collected by a lens and detected by a single-pixel detector [Fig. 2(f)] can be expressed as

$$I_{n,\alpha} = |\mathrm{FFT}\{E_{n,\alpha}(\vec{r}) \cdot O(\vec{r})\}_{\vec{w}=0}|^2$$
$$= \left| \iint P_n(\vec{r}) \cdot O(\vec{r})\mathrm{d}^2\vec{r} + e^{-i\alpha} \iint O(\vec{r})\mathrm{d}^2\vec{r} \right|^2$$
$$= |S_n + e^{-i\alpha}C_2|^2,$$

(3)

where $S_n = \iint P_n(\vec{r}) \cdot O(\vec{r})\mathrm{d}^2\vec{r}$ and $C_2 = \iint O(\vec{r})\mathrm{d}^2\vec{r}$ which is a complex constant.

Then, the complex-valued spectral coefficient of the wavefront can be obtained as
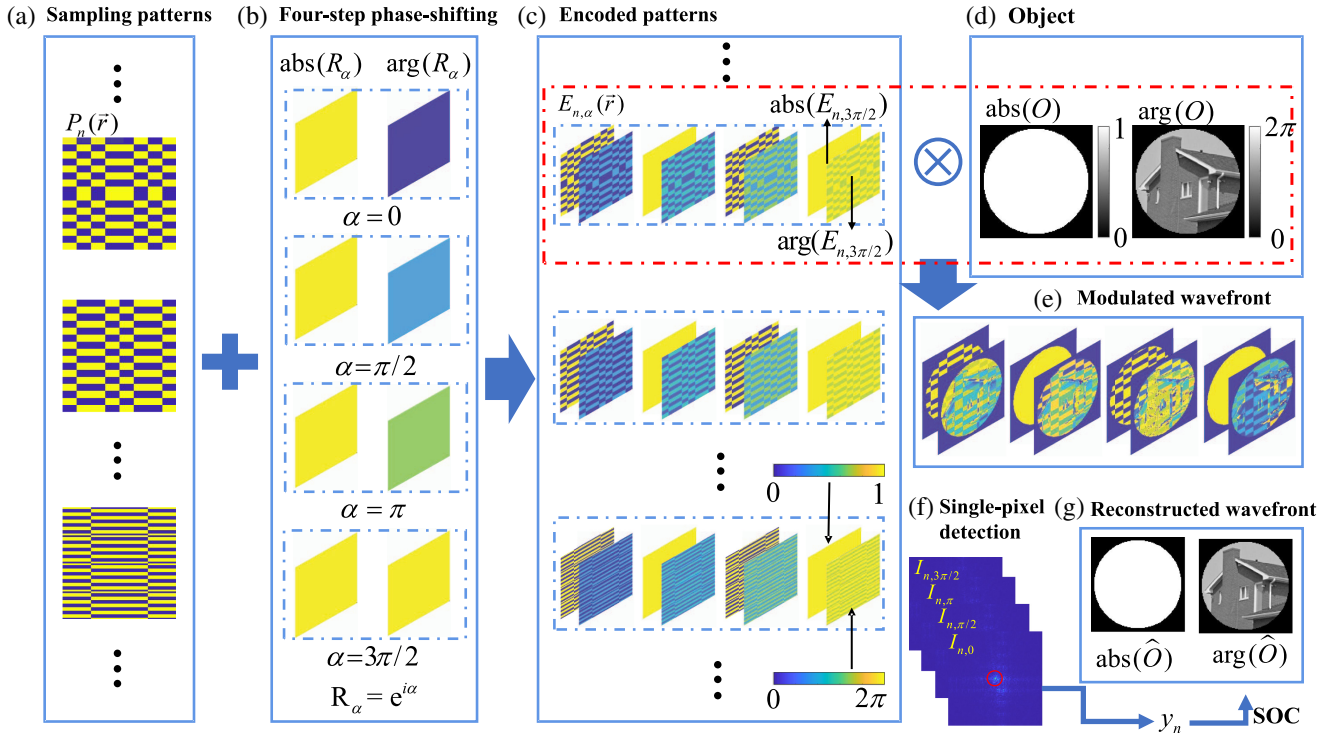

Fig. 2 The schematic diagram of the four-step phase-shifting-based PSSCH method. (a) Sampling patterns; (b) four-step phase shiftings; (c) encoded patterns; (d) target wavefront; (e) modulated wavefront; (f) single-pixel detection; (g) reconstructed wavefront.

$$y_n = \frac{1}{4}\left[(I_{n,0} - I_{n,\pi}) + i\left(I_{n,\frac{\pi}{2}} - I_{n,\frac{3\pi}{2}}\right)\right]. \tag{4}$$

Finally, the reconstruction of the target wavefront $\hat{O}(\vec{r})$ can be obtained via the SOC algorithm

$$\hat{O}(\vec{r}) = \frac{1}{N}\sum_{n=1}^{N} P_n(\vec{r}) \cdot y_n, \tag{5}$$

and the reconstructed amplitude and phase of the wavefront are shown in Fig. 2(g). More details of the mathematical derivation of the method can be seen in Sec. 2 of the Supplementary Material.

3 Experiments and Results

Before conducting experiments, we simulate the proposed PSSCH employing the commonly used Hadamard basis, Fourier basis, and DCT basis for wavefront reconstructions; the results demonstrate the effectiveness of our proposed concept. (The details can be found in Sec. 3 in the Supplementary Material.)

For pursuing a faster modulation speed,[38,51] a DMD-based experimental setup is established (see Sec. 4 in the Supplementary Material). In addition, during the following experiments, the Hadamard basis is selected to demonstrate the effectiveness of the concept, since the Hadamard patterns are binary and can be directly displayed on the binary DMD.

First of all, the USAF 1951 and Siemens star test targets are, respectively, employed to assess the performance of the proposed off-axis-based PSSCH on reconstructing amplitude and phase objects. The reconstructed amplitude of the USAF 1951 test target, as shown in Fig. 3(a), shows the method can resolve group 3, element 1 of the target. The reconstructed phase of the Siemens star target, as shown in Fig. 3(b), confirms

it can achieve high-quality phase reconstruction. To further illustrate the superiority of the proposed method, we compare it with the checkerboard SCH[47–49,51] and peripheral SCH,[41] as shown in Figs. 3(c) and 3(e). It is evident that the proposed method can not only obtain a larger FOV than the peripheral-referenced approach but also achieve a higher imaging resolution than the checkerboard-referenced approach. Due to the different mechanisms of the three reference strategies, half the pixels are used as the reference in the checkerboard reference method, whereas in the peripheral reference and self-reference methods, each pixel serves as the image pixel itself. Consequently, the checkerboard reference displays a lower resolution on the USAF 1951 test target compared to the other two reference strategies.

Next, utilizing the same experimental setup and test targets, we validate the performance of our phase-shifting-based PSSCH. The reconstructed amplitude of the USAF 1951 test target, as shown in Fig. 4(a), shows the method can resolve up to group 3, element 6 of the target. The reconstructed phase of the Siemens star target, as shown in Fig. 4(b), confirms its capability for high-quality phase reconstruction. Compared to the results obtained with the checkerboard SCH in Figs. 4(c) and 4(d), and the peripheral SCH in Figs. 4(e) and 4(f), the same conclusion can be obtained: that our method can not only obtain a larger FOV than the peripheral-referenced approach but also can achieve a higher imaging resolution than the checkerboard-referenced approach.

The results shown in Figs. 3 and 4 suggest that our method can address the trade-off issue suffered by state-of-the-art methods. In addition, the phase-shifting-based PSSCH excels in noise suppression, leading to superior imaging quality compared to the off-axis-based PSSCH. Nonetheless, the off-axis-based PSSCH can avoid the necessary multistep phase-shifting operations in phase-shifting-based PSSCH, and thus it offers
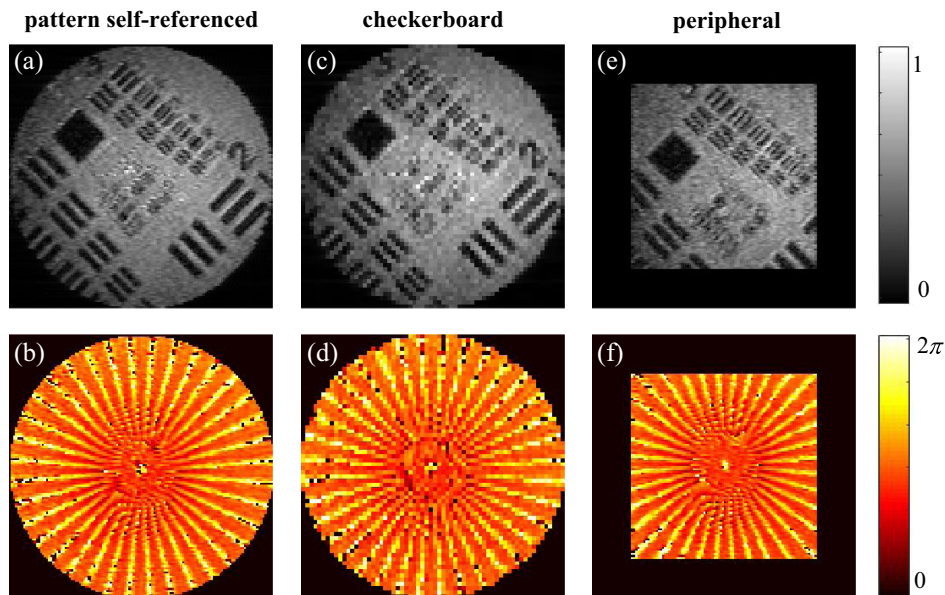

Fig. 3 The amplitude results of the USAF 1951 test target and the phase results of the Siemens star test target reconstructed using the off-axis method. (a), (c), and (e) The reconstructed amplitude by the pattern self-referenced SCH, checkerboard SCH, and peripheral SCH, respectively. (b), (d), and (f) The reconstructed phase by the pattern self-referenced SCH, checkerboard SCH, and peripheral SCH, respectively.

Fig. 4 The amplitude results of the USAF 1951 test target and the phase results of the Siemens star test target reconstructed by the phase-shifting-based method. (a), (c), and (e) The reconstructed amplitude by the pattern self-referenced SCH, checkerboard SCH, and peripheral SCH, respectively. (b), (d), and (f) The reconstructed phase by the pattern self-referenced SCH, checkerboard SCH, and peripheral SCH, respectively.
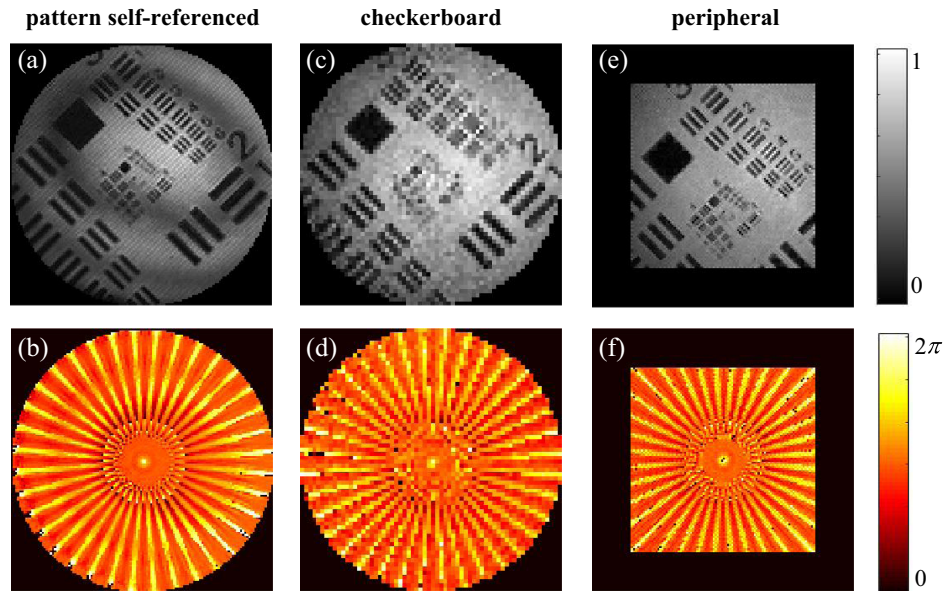
faster imaging speed. The same conclusion can be obtained from the results for the checkerboard SCH and peripheral SCH.

Notably, since it is different from the state-of-the-art methods utilizing a static reference light, our method dynamically introduces the reference light for the single-pixel common-path holographic detection. It thus can suppress dynamically varying noises, which can be noted in Figs. 4(b) and 4(f), reconstructed by the phase-shifting-based PSSCH. However, such merit is not obvious for the phase images reconstructed by the off-axis-

based PSSCH, as shown in Figs. 3(b) and 3(f); this may be because the self-referenced patterns for dynamically introducing the reference light also make the oblique phase grating needed in off-axis-based PSSCH dynamically changing.

Then, to investigate the performance of the proposed method applied in biological imaging, we conduct experiments to do wavefront reconstruction of a biological sample. Here, a dragonfly wing primarily composed of membranes and veins is selected as the target, as shown in Fig. 5(a), of which membranes are thin
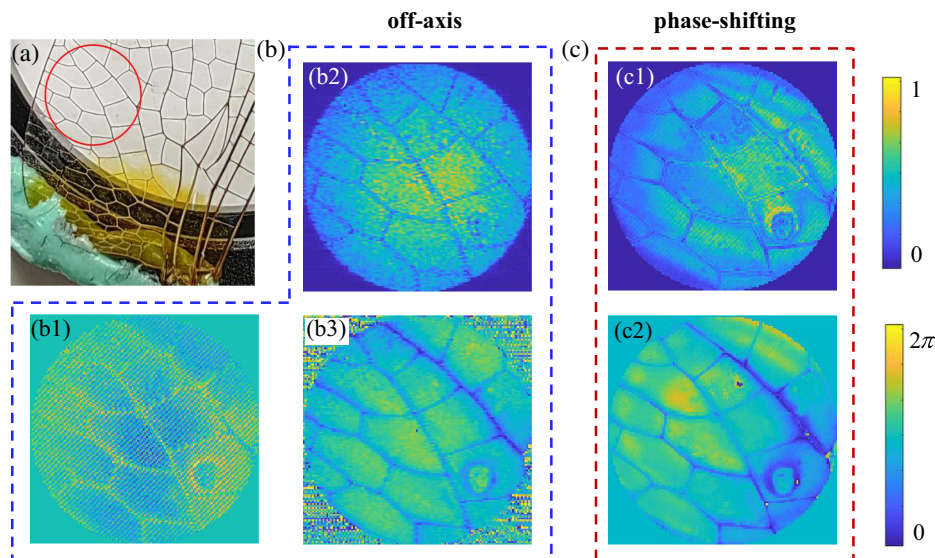

Fig. 5 Experimentally reconstructed wavefront of a dragonfly wing. (a) Photograph of the dragonfly wing. (b) Results of off-axis-based PSSCH method: (b1) off-axis hologram; (b2) and (b3) the reconstructed amplitude and phase, respectively. (c1) and (c2) The amplitude and phase imaging results by phase-shifting-based PSSCH, respectively.

films with high light transmittance, while veins are thicker and have relatively low light transmittance. The reconstructed results of the off-axis-based PSSCH and four-step phase-shifting-based PSSCH are depicted in Figs. 5(b) and 5(c), respectively. It can be seen in Figs. 5(b2) and 5(c1), that the amplitude distributions of the dragonfly wing, reconstructed by the two schemes, exhibit a noticeable contrast between leaf veins and membranes. Moreover, as shown in Figs. 5(b3) and 5(c2), the reconstructed phase distributions also enable a clear distinction between the varying thicknesses of veins and membranes. The results emphasize the effectiveness of the proposed method in reconstructing the amplitude and phase distributions of a dragonfly wing, realized using either the DMD-based off-axis scheme or the DMD-based phase-shifting approach while sharing the same experimental setup. As can be noted in Figs. 5(b) and 5(c), the amplitude and phase of the dragonfly wing reconstructed by the phase-shifting-based PSSCH are a little better than those reconstructed by the off-axis-based PSSCH. However, the off-axis-based PSSCH avoids the need for multiple phase-shifting steps, resulting in imaging speeds that are several times faster. This suggests one can select an appropriate PSSCH to do biomedical imaging.

Finally, we explore the application of the proposed method for lens phase measurement. A physical optical lens with a focal length of 1000 mm, as shown in Fig. 6(a), is measured. The wrapped phase distributions of the measured lens reconstructed by the off-axis-based PSSCH and phase-shifting-based PSSCH are presented in Figs. 6(b) and 6(c), respectively. To illustrate the accuracy of the experimental results, we quantitatively compare the experimental phase profile with the theoretical values. As shown in Figs. 6(d) and 6(e), the solid red lines are the theoretical phase value, the black triangle symbols indicate the experimental values along the dashed lines marked in Figs. 6(b) and 6(c), and the blue dotted lines are the fitting value of the experimental values. The focal length measured by the off-axis-based PSSCH and the phase-shifting-based PSSCH

are on average 998.813 and 999.426 mm, respectively. Comparatively, the accuracy of the off-axis-based PSSCH is slightly inferior to that of the four-step phase-shifting-based PSSCH, consistent with the above experimental conclusion. The results suggest our method has the potential to be effectively applied in phase measurement or defect detection of physical lenses.

4 Discussion

Through the above experiments, we have successfully demonstrated the effectiveness of the proposed PSSCH. It can be implemented using either an off-axis-based scheme or a phase-shifting-based approach, both sharing the same experimental setup. The proposed method utilizes the common basis for single-pixel imaging as the modulation basis, superimposing the necessary multistep phase shifts or an oblique phase grating to sample the wavefront of the unknown light field while introducing the reference light. This enables imaging results with a high imaging resolution comparable to the peripheral-referenced approach while maintaining the FOV as large as that of the checkerboard-referenced approach. In contrast, state-of-the-art methods like the checkerboard-referenced or peripheral-referenced approaches[41,47–49,51] often do not fully utilize pixels, resulting in a reduced imaging FOV or decreased spatial resolution. The imaging results for the USAF 1951 and Siemens star targets confirm that the proposed PSSCH effectively addresses the unavoidable trade-off between imaging FOV and spatial resolution in state-of-the-art methods.

In addition, the proposed PSSCH offers the advantage of dynamically introducing reference light for single-pixel common-path holographic detection, whereas the reference light field in state-of-the-art methods[41,47–49,51] is typically static. The use of dynamic reference light can suppress varying noises, as observed in the images reconstructed by the phase-shifting-
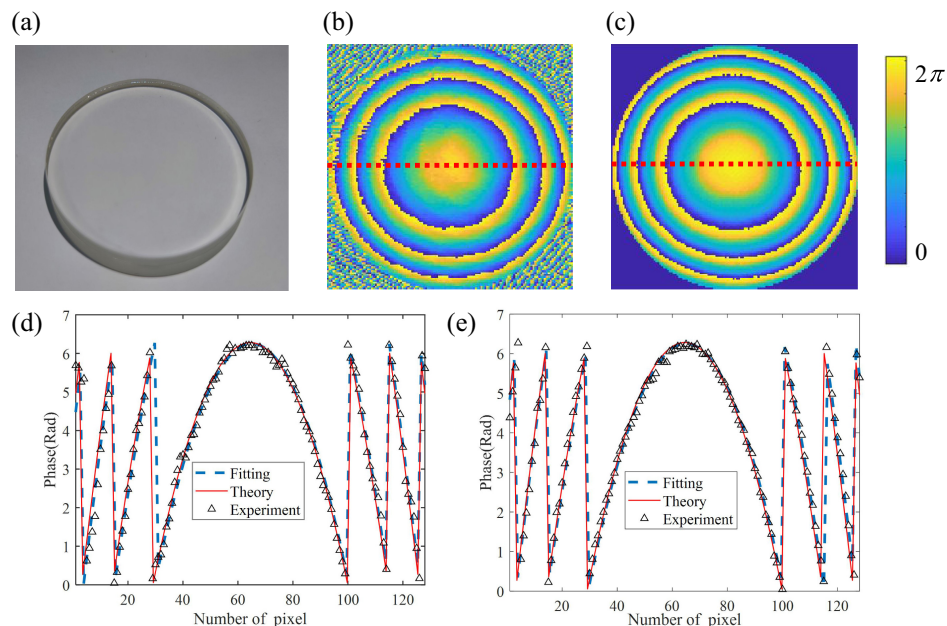

Fig. 6 Experimental measurement results for an optical lens with a focal length of 1000 mm. (a) Physical lens; (b), (c) the wrapped phase distributions measured by off-axis-based and phase-shifting-based PSSCH, respectively. (d), (e) Theoretically and experimentally reconstructed phase profiles along the red dotted lines marked in (b) and (c), respectively.

based PSSCH. However, this benefit is less apparent in the phase images reconstructed by the off-axis-based PSSCH. This may be because the self-referenced patterns used to dynamically introduce the reference light also cause the oblique phase grating, necessary for off-axis-based PSSCH, to change dynamically.

Experimental results show that the phase-shifting-based PSSCH slightly outperforms the off-axis-based PSSCH in imaging fidelity, as expected, due to its superior noise suppression and the lack of limitations on spatial bandwidth products that affect the off-axis-based PSSCH. However, the off-axis-based PSSCH avoids the need for multistep phase-shifting operations, making its imaging speed at least 3 times faster.[51] Therefore, one can flexibly choose between the phase-shifting PSSCH for better imaging fidelity and the off-axis PSSCH for faster imaging speed, depending on the specific requirements.

Finally, while the proposed PSSCH is demonstrated using a DMD-based scheme, it is worth noting that our method could also be implemented using other modulators, such as rotating disks[23,54] or an LCSLM, such as the ferroelectric LCSLM.[55] In addition, the sampling pattern is not restricted to the Hadamard basis used in this work; other modulation bases, such as Fourier basis,[21,26] DCT basis,[47] wavelet basis,[56] or random basis,[44,52] can also be viable alternatives. It should be emphasized that our research results are also applicable to active detection SCH techniques.

5 Conclusion

In summary, we demonstrate a pattern self-referenced single-pixel common-path computational holographic imaging method that can be implemented by either an off-axis scheme or a phase-shifting approach, sharing the same experimental setup. Each pattern is elaborately encoded to serve as a spatial sampling of the target and also introduce reference light for the single-pixel common-path holographic detection. Imaging results of the USAF 1951 and Siemens star targets confirm that the proposed PSSCH can achieve high imaging resolution while maintaining a large FOV compared to state-of-the-art methods. In addition, reconstruction results in biological wavefront imaging and quantitative phase measurement of a physical lens indicate its applicability in various applications.

Disclosures

The authors declare no conflicts of interest.

Code and Data Availability

The data that support the findings of this study are available from the corresponding author upon reasonable request.

References

1. Y. Park, C. Depeursinge, and G. Popescu, "Quantitative phase imaging in biomedicine," *Nat. Photonics* **12**(10), 578–589 (2018).
2. D. Wang et al., "Non-invasive super-resolution imaging through dynamic scattering media," *Nat. Commun.* **12**(1), 3150 (2021).
3. T. Zhang et al., "Noninvasive imaging through scattering media with enlarged FOV using PSF estimations and correlations," *Adv. Photonics Res.* **4**, 2300100 (2023).
4. Y. L. Li et al., "Tunable liquid crystal grating based holographic 3D display system with wide viewing angle and large size," *Light: Sci. Appl.* **11**(1), 188 (2022).
5. D. Wang et al., "Holographic capture and projection system of real object based on tunable zoom lens," *PhotoniX* **3**, 1–15 (2020).
6. C. Liu et al., "Continuous optical zoom microscope with extended depth of field and 3D reconstruction," *PhotoniX* **3**(1), 20 (2022).
7. D. Gabor, "Microscopy by reconstructed wave-fronts," *Proc. R. Soc. A* **197**(1051), 454–487 (1949).
8. R. F. Vanligten and H. Osterberg, "Holographic microscopy," *Nature* **211**(5046), 282–283 (1966).
9. R. Bousso, "The holographic principle for general backgrounds," *Classical Quantum Gravity* **17**(5), 997 (2000).
10. J. Rosen and G. Brooker, "Non-scanning motionless fluorescence three-dimensional holographic microscopy," *Nat. Photonics* **2**(3), 190–195 (2008).
11. Y. Baek et al., "Kramers-Kronig holographic imaging for high-space-bandwidth product," *Optica* **6**(1), 45–51 (2019).
12. Z. Huang and L. Cao, "High bandwidth-utilization digital holographic multiplexing: an approach using Kramers-Kronig relations," *Adv. Photonics Res.* **3**(2), 2100273 (2019).
13. Y. Gao and L. Cao, "Iterative projection meets sparsity regularization: towards practical single-shot quantitative phase imaging with in-line holography," *Light: Adv. Manuf.* **4**(1), 37–53 (2023).
14. Z. Huang et al., "Dual-plane coupled phase retrieval for non-prior holographic imaging," *PhotoniX* **3**(1), 1–16 (2022).
15. P. Ferraro et al., "Compensation of the inherent wave front curvature in digital holographic coherent microscopy for quantitative phase-contrast imaging," *Appl. Opt.* **42**(11), 1938–1946 (2003).
16. S. Grilli et al., "Whole optical wavefields reconstruction by digital holography," *Opt. Express* **9**(6), 294–302 (2001).
17. Z. Yang et al., "Generalized Hartmann-Shack array of dielectric metalens sub-arrays for polarimetric beam profiling," *Nat. Commun.* **9**(1), 4607 (2018).
18. L. Zha et al., "Single-pixel tracking of fast-moving object using geometric moment detection," *Opt. Express* **29**(19), 30327–30336 (2021).
19. O. Katz, Y. Bromberg, and Y. Silberberg, "Compressive ghost imaging," *Appl. Phys. Lett.* **95**, 131110 (2009).
20. M. P. Edgar, G. M. Gibson, and M. J. Padgett, "Principles and prospects for single-pixel imaging," *Nat. Photonics* **13**(1), 13–20 (2019).
21. B. Sun et al., "3D computational imaging with single-pixel detectors," *Science* **340**(6134), 844–847 (2013).
22. Z. Zhang, X. Ma, and J. Zhong, "Single-pixel imaging by means of Fourier spectrum acquisition," *Nat. Commun.* **6**(1), 6225 (2015).
23. E. Hahamovich et al., "Single pixel imaging at megahertz switching rates via cyclic Hadamard masks," *Nat. Commun.* **12**(1), 4516 (2021).
24. X. Zhang et al., "VGenNet: variable generative prior enhanced single pixel imaging," *ACS Photonics* **10**, 2363–2373 (2023).
25. D. Franklin et al., "Actively addressed single pixel full-colour plasmonic display," *Nat. Commun.* **8**(1), 15209 (2017).
26. W. Yang et al., "Anti-motion blur single-pixel imaging with calibrated radon spectrum," *Opt. Lett.* **47**(12), 3123–3126 (2022).
27. G. M. Gibson, S. D. Johnson, and M. J. Padgett, "Single-pixel imaging 12 years on: a review," *Opt. Express* **28**(19), 28190–28208 (2020).

28. N. Radwell et al., "Single-pixel infrared and visible microscope," *Optica* **3**(5), 285–289 (2014).
29. M. J. Sun et al., "Single-pixel three-dimensional imaging with time-based depth resolution," *Nat. Commun.* **7**(1), 12010 (2016).
30. Y. Wang et al., "Mid-infrared single-pixel imaging at the single-photon level," *Nat. Commun.* **14**(1), 1073 (2023).
31. B. Zeng et al., "Hybrid graphene metasurfaces for high-speed mid-infrared light modulation and single-pixel imaging," *Light: Sci. Appl.* **7**(1), 51 (2018).
32. R. I. Stantchev et al., "Real-time terahertz imaging with a single-pixel detector," *Nat. Commun.* **11**(1), 2535 (2020).
33. W. Li et al., "Dual-color terahertz spatial light modulator for single-pixel imaging," *Light: Sci. Appl.* **11**(1), 191 (2022).
34. R. I. Stantchev et al., "Noninvasive, near-field terahertz imaging of hidden objects using a single-pixel detector," *Sci. Adv.* **2**(6), e1600190 (2016).
35. M. P. Olbinado et al., "X-ray phase-contrast ghost imaging using a single-pixel camera," *Optica* **8**(12), 1538–1544 (2021).
36. D. Wu et al., "Imaging biological tissue with high-throughput single-pixel compressive holography," *Nat. Commun.* **12**(1), 4712 (2021).
37. P. Clemente et al., "Compressive holography with a single-pixel detector," *Opt. Lett.* **38**(14), 2524–2527 (2013).
38. H. González et al., "High sampling rate single-pixel digital holography system employing a DMD and phase-encoded patterns," *Opt. Express* **26**(16), 20342–20350 (2018).
39. L. Martínez-León et al., "Single-pixel digital holography with phase-encoded illumination," *Opt. Express* **25**(5), 4975–4984 (2017).
40. H. Y. Hou et al., "Complex-amplitude single-pixel imaging using coherent structured illumination," *Opt. Express* **29**(25), 41827–41841 (2021).
41. K. Ota and Y. Hayasaki, "Complex-amplitude single-pixel imaging," *Opt. Lett.* **43**(15), 3682–3685 (2018).
42. L. Gao et al., "OAM-basis wavefront single-pixel imaging via compressed sensing," *J. Lightwave Technol.* **41**(7), 2131–2137 (2022).
43. X. Li et al., "Quantitative imaging for optical field via a single-pixel detector," *Signal Process.* **188**, 108173 (2021).
44. N. Yoneda, Y. Saita, and T. Nomura, "Common-path off-axis single-pixel holographic imaging," *Opt. Express* **30**(11), 18134–18144 (2022).
45. P. He et al., "Wavefront single-pixel imaging using a flexible SLM-based common-path interferometer," *Opt. Lasers Eng.* **168**, 107633 (2023).
46. Y. Liu et al., "Single-pixel phase and fluorescence microscope," *Opt. Express* **26**(25), 32451–32462 (2018).
47. S. Sun et al., "DCT single-pixel detecting for wavefront measurement," *Opt. Laser Technol.* **163**, 109326 (2023).
48. R. Liu et al., "Complex wavefront reconstruction with single-pixel detector," *Appl. Phys. Lett.* **114**, 161901 (2019).
49. S. Zhao et al., "Fourier single-pixel reconstruction of a complex amplitude optical field," *Opt. Lett.* **44**(13), 3278–3281 (2019).
50. Y. Liu et al., "Single-pixel spiral phase contrast imaging," *Opt. Lett.* **45**(14), 4028–4031 (2020).
51. Z. Du et al., "DMD-based single-pixel off-axis interferometry for wavefront reconstruction of a biological sample," *Appl. Phys. Lett.* **123**, 033702 (2023).
52. M. Li et al., "Single-pixel ptychography," *Opt. Lett.* **46**(7), 1624–1627 (2021).
53. M. Takeda, H. Ina, and S. Kobayashi, "Fourier-transform method of fringe-pattern analysis for computer-based topography and interferometry," *JOSA* **72**(1), 156–160 (1982).
54. W. Jiang et al., "Single-pixel camera based on a spinning mask," *Opt. Lett.* **46**(19), 4859–4862 (2021).
55. D. Armitage et al., "Ferroelectric liquid crystal spatial light modulator," *Mol. Cryst. Liq. Cryst.* **144**(5), 309–316 (1987).
56. M. Alemohammad et al., "High-speed all-optical Haar wavelet transform for real-time image compression," *Opt. Express* **25**(9), 9802–9811 (2017).

Wenjing Zhao is currently an assistant professor at the Taiyuan University of Technology, Taiyuan, China. She received her PhD from Sichuan University, Chengdu, China. Her research interests include optical imaging and optical sensing.

Zefang Gao received the BSc degree from the Taiyuan University of Technology, Taiyuan, China, in 2022, where she is currently working toward the BEng degree. Her research focuses on new sensing and imaging.

Zhiheng Du received the BSc degree from the Institutes of Technology of Henan, Henan, China, in 2021, where he is currently working toward the BEng degree. His research focuses on new sensing and imaging.

Aiping Zhai is currently an assistant professor at Taiyuan University of Technology, Taiyuan, China. She received her PhD from Sichuan University, Chengdu, China. Her research interests include optical imaging and optical sensing.

Dong Wang received his PhD in instrument science and technology from Harbin Institute of Technology, Harbin, China, in 2013. He is a professor at the College of Physics and Optoelectronics, Taiyuan University of Technology, Taiyuan, China, and the Key Laboratory of Advanced Transducers and Intelligent Control Systems, Ministry of Education, Taiyuan University of Technology. His research interests include optical sensing, optical imaging, and optical engineering.